Comprehensive Study on Structure−Activity Relationships of Rifamycins: Discussion of Molecular and Crystal Structure and Spectroscopic and Thermochemical Properties of Rifamycin O

Alessia Bacchi* and Giancarlo Pelizzi

Dipartimento di Chimica Generale ed Inorganica, Chimica Analitica, Chimica Fisica, Università di Parma, viale delle Scienze, I-43100 Parma, Italy

Marino Nebuloni† and Pietro Ferrari

Biosearch Italia S.p.A., Via Lepetit, 34, I-21040 Gerenzano, Italy

Received November 20, 1997

The mechanism of action of rifamycins against bacterial DNA-dependent RNA polymerase has been explained on the basis of the spatial arrangement of four oxygens which can form hydrogen bonds with the enzyme. Structural descriptors are derived from X-ray diffraction crystal structures of 25 active and nonactive rifamycins. Principal component analysis is used to find the combination of structural parameters which better discriminate between active and nonactive rifamycins. Two possible mechanisms of molecular rearrangement are described which can convert nonactive into active conformations. The energy involved for conformational rearrangements is studied by molecular modeling techniques. Methyl C34 is found to play a key role for determining the geometry of the pharmacophore. Rifamycin O, reported to be active, is obtained by oxidation of rifamycin B and is studied by X-ray single-crystal diffractometry, by solution IR and NMR spectroscopy, and by thermal analysis. Surprisingly the oxidation process is totally stereospecific, and an explanation is given based on solution spectroscopic evidence. The conformation found in the solid state is typical of nonactive compounds, and molecular mechanics calculations show that a molecular rearrangement to the active conformation would require about 15 kcal/mol. Thermal analysis confirms that rifamycin O has a sterically constrained conformation. Therefore, it is likely that the antibiotic activity of rifamycin O is due either to chemical modification prior to reaching the enzyme or to conformational activation.

Introduction

Rifamycins are antibiotics belonging to the group of naphthalenic ansamycins which exert their activity by specific inhibition of bacterial DNA-dependent RNA polymerase (DDRP). They have activity against a large variety of organisms, such as bacteria, eukaryotes, and viruses, and for this reason they are sometimes called "wonder drugs".[1] A large variety of rifamycin derivatives have been studied during the last 30 years. The molecule is made by a naphthoquinonic system condensed to a furanone ring (chromophore) spanned by a 17-membered ansa chain connecting two opposite sides of the chromophore.

In the present work the crystal structure of rifamycin O (4-*O*-(carboxymethyl)-1-deoxy-1,4-dihydro-4-hydroxy-1-oxorifamycin γ-lactone) is described. Rifamycin O is an antibiotic rifamycin derivative obtained by the oxidation of natural rifamycin B produced from *Streptomyces mediterranei*. The oxidation from rifamycin B to rifamycin O originates a new chiral center and should give a mixture of diastereoisomers (Scheme 1). Surprisingly, it turns out that the reaction is totally stereospecific and involves a nucleophilic attack occurring at the most sterically hindered side of the chromophore. A mechanism for the oxidation is proposed on the basis of solution IR and NMR evidence and on the basis of the crystal structure of rifamycin B *p*-iodoanilide[2] and rifamycin O.

A phenomenological model based on chemical evidence has been developed[1] to explain the mechanism of action of rifamycins. It involves the formation of hydrogen bonds between the enzyme and four rifamycin oxygens, which must be arranged in an unspecified favorable three-dimensional pattern. The direct structural characterization of this pattern is not available since neither the structure of the complex between rifamycin and DDRP nor that of isolated DDRP has ever been determined. In the absence of first-hand information on the mode of interaction between rifamycins and DDRP, several studies have related the solid-state structure of rifamycins to the conditions needed for activity.[3−8] A qualitative structural model describing the three-dimensional organization of the pharmacophore has been developed[5] on the basis of crystal structures and is currently generally accepted (Chart 1).

The present work provides a quantitative characterization of this model by performing a multivariate statistical analysis on the conformational parameters of all rifamycin molecules whose crystal structures are known. The rationale for this investigation is based on

* Corresponding author.
† Present address: REDOX, Via S. Margherita, 51, I-20093 Cologno Monzese, Italy.

S0022-2623(97)00791-7 CCC: $15.00
Published on Web 05/23/1998

Scheme 1

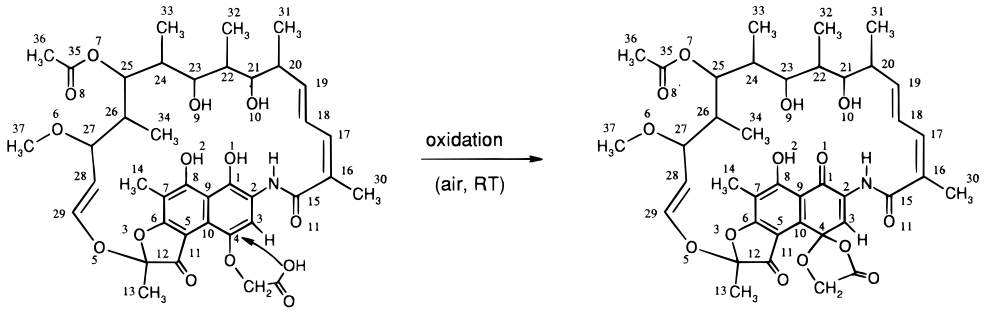

Rifamycin B Rifamycin O

Chart 1

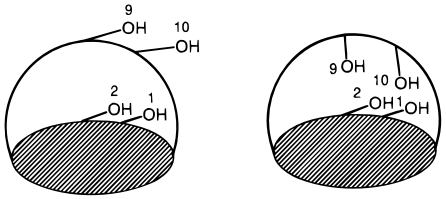

the principles of structure correlation[9,10] which can be summarized as follows:

(1) The crystal field experienced by rifamycins in the solid state is qualitatively similar to the forces acting on the molecule in organized environments such as in solution, or in the interaction with DDRP.

(2) The collection of geometries that different rifamycin derivatives or polymorphs adopt in different crystalline environments provides a mapping of low-energy conformations accessible to rifamycins in solution or when interacting with DDRP. The ensemble of crystal structures is considered as a sampling of the conformational energy hypersurface in proximity of minima.

(3) Principal Component Analysis is applied on structural parameters to highlight the directions of larger spread of the conformations on the hypersurface. If active and nonactive rifamycins are grouped in separate clusters along these directions, then it is conceivable that the conformational preorganization of active rifamycins cannot be significantly altered by the forces present in solution.

(4) The analysis of the structural parameters which mostly determine the separation provides indications on the principal steric requisites of the pharmacophore.

In the present work the crystal structure of rifamycin O is determined and compared to other rifamycins on the basis of the above procedure. It is found that the crystal conformation of rifamycin O should not be able to inhibit DDRP, in complete contrast with activity data reported.[1] This could be due either to a conformational rearrangement of rifamycin O in solution or to a chemical modification of the molecule before interacting with DDRP. A mechanism for the rearrangement of rifamycin O from nonactive to active conformation is discussed, and the energy involved is examined by molecular modeling methods, by solid-state crystallographic and thermal analysis, and by solution IR and NMR studies.

Results and Discussion

Crystal Structure of Rifamycin O. Final atomic coordinates relative to the structure refinement are in Table 1, whereas geometric parameters are in Table 2. Figure 1 shows a perspective view of rifamycin O along with the labeling scheme. The molecule can be described in terms of the chromophore, comprising atoms from C1 to C12 and from O1 to O4; the ansa chain, involving atoms from C15 to C29, N, and O5; and finally the dioxolanone substituent at C4, formed by O12, O13, O14, C38, and C39. The chromophore is joined to the ansa through an amidic junction at C2 and an etheric junction at C12. The chromophore is planar within 0.17 Å and forms a dihedral angle of 69° with the average plane of the ansa chain backbone, whose atoms deviate from planarity by values up to 1.2 Å. The overall inclination of the ansa on the chromophore varies continuously from 64° to 124° for active rifamycins, while it can be less than 50° for nonactive compounds.[6,11,12] The amidic junction is planar (C1−C2−N−C15 = 174.2(5)° and C2−N−C15−O11 (T1) = 9.5 (5)°), and O11 is oriented on the opposite side of the C2−N bond with respect to O1. This arrangement favors the occurrence of two intramolecular hydrogen bonds: N−H···O1 (N···O1 = 2.629(5) Å, N−H···O1 = 108(1)°) and C3−H···O11 (C3···O11 = 2.855(6) Å, C3−H···O11 = 123(1)°). The conformation of the etheric junction is characterized by the torsion angles C12−O5−C29−C28 (T16) = 65.8(5)° and O3−C12−O5−C29 (T17) = −81.6(7)°. Both junctions have geometries comparable with those found in active rifamycins. The conformation of the central section of the ansa chain from C20 to C25 influences the orientation of vectors C23−O9 and C21−O10, which are important for the structural organization of the pharmacophore. For rifamycin O torsion angles C19−C20−C21−C22 (T7), C20−C21−C22−C23 (T8), C21−C22−C23−C24 (T9), and C22−C23−C24−C25 (T10) are −172.6(5)°, −172.0 (6)°, 63.2(7)°, and 177.9(5)°, respectively, in good agreement with those found for active rifamycins. On the contrary, interatomic distances among the four oxygens O1, O2, O9, and O10 constituting the pharmacophore are O1···O9 = 4.300(7), O1···O10 = 2.912(9), O2···O9 = 3.612(7), and O2···O10 = 3.980(7) Å, while in active compounds they range between 5.41 and 9.58 Å. This discrepancy is explained by a rigid rotation of the C20−C25 section of the ansa chain around the bonds C19−C20 (C18−C19−C20−C21 = 117.4(8)°) and C26−C27 (C25−C26−C27−C28 = 56.0(7)°), which in rifamycin O

Table 1. Fractional Atomic Coordinates ($\times 10^4$) and Equivalent Isotropic Displacement Parameters ($Å^2 \times 10^4$)[a]

atom	*X*/*a*	*Y*/*b*	*Z*/*c*	U_{eq}
O1	6835(3)	−2870(4)	7301(4)	526(16)
O2	7742(4)	−2482(5)	9893(5)	638(19)
O3	11344(3)	1828(4)	10019(5)	583(19)
O4	11982(4)	3682(5)	6154(5)	694(20)
O5	12617(4)	4364(5)	9034(5)	671(22)
O6	9711(3)	6269(4)	8991(5)	600(19)
O7	7439(3)	3940(4)	8902(4)	508(16)
O8	8548(4)	2706(5)	10812(5)	643(19)
O9	6622(4)	581(4)	8531(5)	568(18)
O10	5454(5)	−881(6)	6450(6)	833(31)
O11	6603(4)	−616(5)	1769(5)	727(20)
O12	10578(3)	1288(4)	4666(5)	530(17)
O13	9453(3)	2687(4)	4493(4)	485(15)
O14	10543(5)	4864(6)	2868(7)	923(28)
N	6431(4)	−1945(4)	4283(5)	487(18)
C1	7575(4)	−1622(5)	6660(5)	419(20)
C2	7483(4)	−1013(5)	4972(5)	418(20)
C3	8335(4)	270(5)	4229(6)	450(21)
C4	9438(4)	1170(5)	5063(5)	413(20)
C5	10418(5)	1458(6)	7678(6)	454(21)
C6	10379(5)	956(6)	9269(6)	471(23)
C7	9494(5)	−347(6)	10059(6)	499(24)
C8	8590(5)	−1187(6)	9169(6)	480(23)
C9	8569(5)	−696(5)	7544(5)	398(19)
C10	9476(4)	631(5)	6794(5)	407(19)
C11	11543(5)	2800(6)	7332(7)	531(25)
C12	12239(5)	2943(7)	8918(7)	548(26)
C13	13407(7)	2581(10)	9280(10)	850(44)
C14	9493(7)	−880(8)	11766(7)	729(35)
C15	6009(5)	−1675(6)	2778(6)	493(22)
C16	4802(5)	−2861(6)	2404(6)	576(24)
C17	3725(6)	−3171(7)	2891(7)	706(30)
C18	3486(6)	−2473(8)	3794(8)	725(31)
C19	3979(6)	−1056(7)	3730(7)	629(28)
C20	3700(6)	−426(9)	4738(9)	719(34)
C21	4880(5)	214(6)	5722(7)	530(24)
C22	4665(5)	703(6)	6943(7)	542(25)
C23	5895(5)	1540(6)	7761(6)	491(23)
C24	6738(5)	3029(6)	6748(6)	486(22)
C25	7910(5)	3761(6)	7745(6)	488(22)
C26	8813(5)	5297(6)	6878(6)	531(24)
C27	10030(5)	5920(6)	7880(7)	576(27)
C28	10777(6)	4882(7)	8648(7)	613(27)
C29	11864(6)	5215(7)	8305(8)	617(28)
C30	4918(7)	−3642(8)	1449(9)	813(37)
C31	3134(10)	750(14)	3773(13)	1304(83)
C32	3824(7)	−614(8)	8122(10)	829(38)
C33	6030(6)	4097(7)	5811(8)	703(31)
C34	9175(7)	5253(8)	5467(8)	713(33)
C35	7824(5)	3365(6)	10377(7)	545(23)
C36	7272(7)	3676(9)	11400(8)	773(37)
C37	10751(6)	7259(8)	9652(8)	697(33)
C38	11011(6)	2661(7)	3456(7)	630(28)
C39	10366(5)	3575(6)	3502(6)	551(23)

[a] One-third trace of the diagonalized matrix, with s.u.'s in parentheses for non-hydrogen atoms.

Table 2. Bond Distances (Å) and Angles (deg)[a]

O1−C1	1.228(5)	N−C2	1.405(6)	C17−C18	1.459(14)
O2−C8	1.331(6)	N−C15	1.346(6)	C18−C19	1.316(11)
O3−C6	1.358(6)	C1−C2	1.470(7)	C19−C20	1.513(14)
O3−C12	1.459(6)	C1−C9	1.477(7)	C20−C21	1.515(8)
O4−C11	1.204(7)	C2−C3	1.332(6)	C20−C31	1.513(16)
O5−C12	1.390(9)	C3−C4	1.491(6)	C21−C22	1.545(11)
O5−C29	1.389(9)	C4−C10	1.510(7)	C22−C23	1.535(7)
O6−C27	1.416(10)	C5−C6	1.398(7)	C22−C32	1.526(9)
O6−C37	1.415(8)	C5−C10	1.401(7)	C23−C24	1.525(6)
O7−C25	1.455(9)	C5−C11	1.453(6)	C24−C25	1.548(7)
O7−C35	1.333(6)	C6−C7	1.376(6)	C24−C33	1.537(10)
O8−C35	1.212(9)	C7−C8	1.394(7)	C25−C26	1.530(6)
O9−C23	1.451(8)	C7−C14	1.495(8)	C26−C27	1.546(8)
O10−C21	1.427(10)	C8−C9	1.421(7)	C26−C34	1.530(12)
O11−C15	1.219(6)	C9−C10	1.387(6)	C27−C28	1.531(10)
O12−C4	1.434(7)	C11−C12	1.553(9)	C28−C29	1.275(10)
O12−C38	1.419(6)	C12−C13	1.505(12)	C35−C36	1.492(13)
O13−C4	1.446(6)	C15−C16	1.508(7)	C38−C39	1.467(12)
O13−C39	1.377(7)	C16−C17	1.332(10)		
O14−C39	1.182(7)	C16−C30	1.495(13)		

C6−O3−C12	107.9(5)	C2−N−C15	127.9(4)
C12−O5−C29	119.9(5)	O1−C1−C2	120.0(4)
C27−O6−C37	113.3(5)	O1−C1−C9	121.7(5)
C25−O7−C35	118.1(4)	C2−C1−C9	118.3(4)
C4−O12−C38	108.1(4)	N−C2−C1	112.3(4)
C4−O13−C39	108.5(4)	N−C2−C3	125.8(5)
C1−C2−C3	121.9(4)	O3−C12−O5	110.9(5)
C2−C3−C4	121.9(5)	O3−C12−C11	104.6(4)
O12−C4−O13	105.5(4)	O3−C12−C13	109.7(6)
O12−C4−C3	109.8(4)	O5−C12−C11	114.4(5)
O12−C4−C10	109.2(4)	O5−C12−C13	106.4(6)
O13−C4−C3	107.7(4)	C11−C12−C13	111.0(6)
O13−C4−C10	107.7(4)	O11−C15−N	122.9(5)
C3−C4−C10	116.4(4)	O11−C15−C16	121.5(5)
C6−C5−C10	119.1(5)	N−C15−C16	115.4(5)
C6−C5−C11	106.8(5)	C15−C16−C17	121.9(6)
C10−C5−C11	134.1(5)	C15−C16−C30	114.7(5)
O3−C6−C5	114.3(4)	C17−C16−C30	123.4(6)
O3−C6−C7	121.2(5)	C16−C17−C18	128.6(7)
C5−C6−C7	124.4(5)	C17−C18−C19	128.5(7)
C6−C7−C8	115.8(6)	C18−C19−C20	125.2(7)
C6−C7−C14	123.4(5)	C19−C20−C21	110.6(6)
C8−C7−C14	120.8(5)	C19−C20−C31	110.7(8)
O2−C8−C7	117.8(5)	C21−C20−C31	110.9(7)
O2−C8−C9	120.5(5)	O10−C21−C20	108.2(6)
C7−C8−C9	121.7(5)	O10−C21−C22	110.0(5)
C1−C9−C8	119.3(4)	C20−C21−C22	114.6(5)
C1−C9−C10	120.2(5)	C21−C22−C23	113.0(5)
C8−C9−C10	120.5(4)	C21−C22−C32	112.2(6)
C4−C10−C5	121.0(4)	C23−C22−C32	110.2(6)
C4−C10−C9	120.6(4)	O9−C23−C22	109.7(5)
C5−C10−C9	118.4(5)	O9−C23−C24	108.2(4)
O4−C11−C5	133.5(6)	C22−C23−C24	116.0(5)
O4−C11−C12	121.1(5)	C23−C24−C25	109.8(5)
C5−C11−C12	105.3(5)	C23−C24−C33	112.2(5)
		C25−C24−C33	111.7(5)
O7−C25−C24	106.1(4)	C27−C28−C29	122.7(7)
O7−C25−C26	108.3(4)	O5−C29−C28	125.1(7)
C24−C25−C26	115.2(5)	O7−C35−O8	124.0(6)
C25−C26−C27	113.6(5)	O7−C35−C36	111.0(5)
C25−C26−C34	111.3(5)	O8−C35−C36	125.0(7)
C27−C26−C34	108.4(5)	O12−C38−C39	105.0(5)
O6−C27−C26	108.3(5)	O13−C39−O14	121.0(6)
O6−C27−C28	110.9(5)	O13−C39−C38	108.9(5)
C26−C27−C28	114.6(5)	O14−C39−C38	130.1(6)

[a] With s.u.'s in parentheses.

moves O9 and O10 toward the chromophore. The mechanism is probably favored by a conformational rearrangement around C17−C18 (C16−C17−C18−C19 = 36(1)°) and will be discussed in the following section. In fact the distribution of the 17 torsion angles defining the ansa chain backbone observed for crystals of active rifamycins, Figure 2a, shows that the maximum differentiation of conformation of the ansa chain between rifamycin O and active compounds is at C16−C17−C18−C19 (T4), C18−C19−C20−C21 (T6), and C25−C26−C27−C28 (T13), while the geometry of the central segment (T7, T8, T9, T10) is practically the same. For active rifamycins, the distribution of torsion angles at the two junctions, T1, T2, T16, and T17, is spread, bimodal in the case of T16, according to local flexibility and multiple conformations observed in solution.[13] Figure 2b reports the torsion angles found in crystals of nonactive rifamycins. Compared to Figure 2a, values are more scattered, indicating that nonactive molecules do not possess a common structural pattern. In some cases T6 and T13 are similar to those found for rifamycin O.

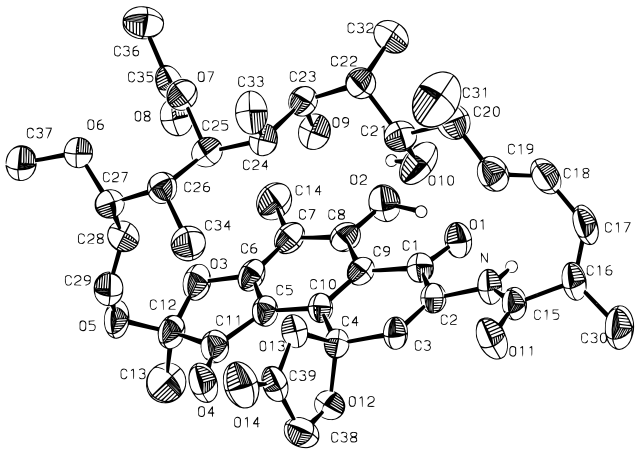

Figure 1. ORTEP view of rifamycin O. Thermal displacement ellipsoids are drawn at 50% probability level. Hydrogens not relevant for the discussion have been omitted for clarity.

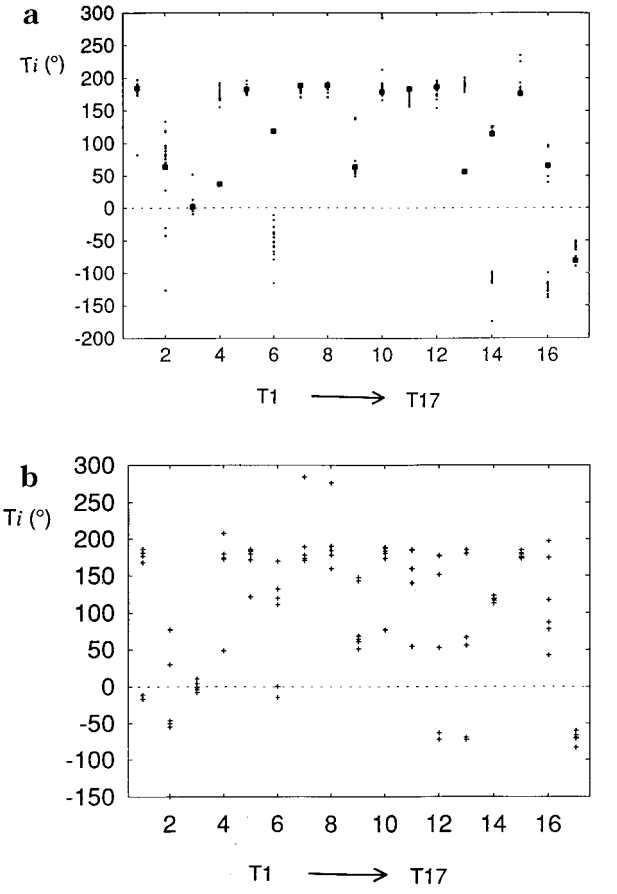

Figure 2. See text for numbering of torsion angles. (a) Comparison of torsion angles along the ansa chain from T1 to T17 between crystalline active rifamycins (●) and rifamycin O (■). Major discrepancies are observed at T4, T6, and T13. (b) Distribution of torsion angles along the ansa chain from T1 to T17 for crystalline nonactive rifamycins. The values are more scattered than above, indicating the lack of a common structural pattern.

The glycolic group is oriented with the C=O pointing toward the ansa chain; consequently the absolute configuration at C4 is *R*. The five-membered ring is planar within 0.13 Å and results nearly perpendicular (87°) to the chromophore. The role of the dioxolanone ring on the conformational features of rifamycin O is discussed in the next section.

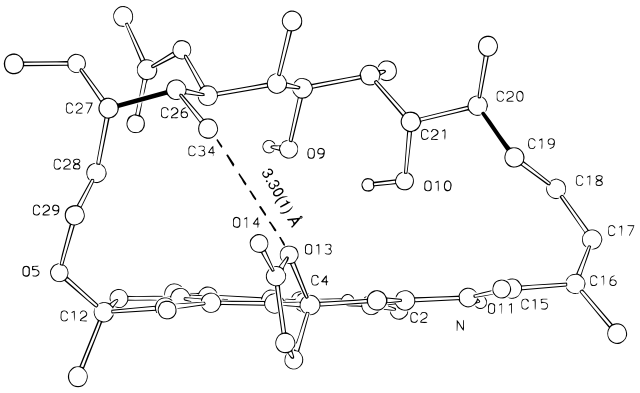

Figure 3. View of the molecular structure of rifamycin O as found in the crystal, showing the short contact between C34 and the glycolic ring. Bonds corresponding to torsion angles T6 (C18−C19−C20−C21) and T13 (C25−C26−C27−C28) are highlighted. In the discussion we suggest that, by removing the hindrance of the glycolic group, the central part of the ansa chain might rotate around the two hinges at T6 and T13 and restore the conditions required for activity.

O1 and O2 are involved in a strong intramolecular hydrogen bond (O1···O2 = 2.537(6) Å, O1···H−O2 = 161(9)°), as well as O9 and O10 (O10···O9 = 2.703(8) Å, O10−H···O9 = 149(6)°). O9 participates to the only intermolecular hydrogen bond occurring in the crystal packing (O9···O11(x,y,z+1) = 2.834(6) Å, O9−H···O11 = 175(9)°).

Influence of Methyl C34 on the Conformation of the Ansa Chain. Methyl C34 is the point at which the ansa chain and the chromophore come into closest contact, typically C34−C10 = 3.37−3.87 Å. In rifamycin O the approach of methyl C34 to the quinonic nucleus is hindered by the five-membered ring substituted at C4, which lies approximately perpendicular to the chromophore plane, giving rise to a fairly short repulsive interaction, C34···O13 = 3.30(1) Å, and C34···C10 is forced to elongate to 4.61(1) Å, Figure 3. This contact affects the torsion angle T13 and may be considered responsible for the bending of the central section of the ansa chain found in rifamycin O. As previously discussed, the difference between the conformation of rifamycin O and of other active rifamycins is particularly due to torsion angles T13, T6, and T4. The rotation around C26−C27, described by T13, is in principle sufficient to move O9 and O10 away from the chromophore, switching the central part of the ansa chain from a nonactive to an active pattern. The corresponding conformational rearrangement for rifamycin O has been simulated by increasing T13 in steps of 10° and minimizing the structure at each step. Figure 4 shows three intermediate conformations from T13 = 60°, corresponding to the geometry found in the crystal, to T13 = 200°, which is typical of active rifamycins. The energy profile of the complete rotation around the C26−C27 bond, Figure 5(top), solid line, shows that the crystal conformation sits in a deep minimum, while the local minimum corresponding to the conformation characteristic of active compounds is higher in energy and remarkably shallow (in fact it resembles an inflection point). The activation energy for the conversion from nonactive to active conformation is about 12 kcal/mol and corresponds to the passage of methyl C34 closest to the chromophore. The reverse

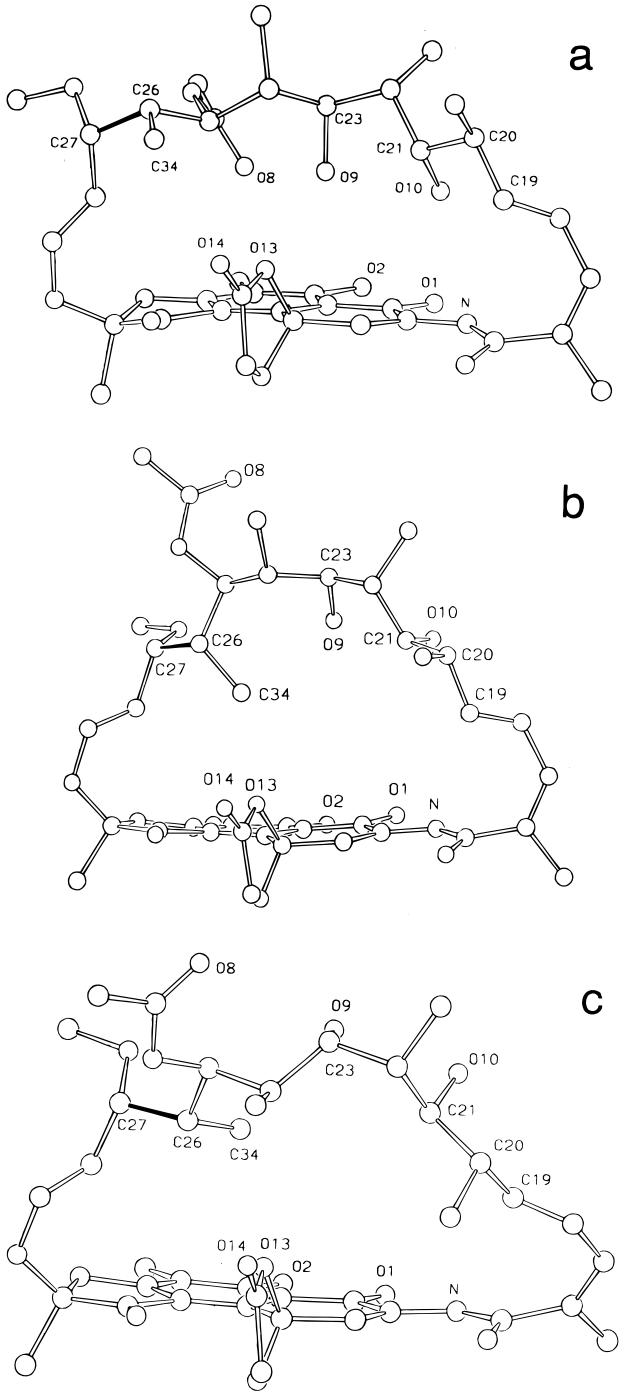

Figure 4. Three steps of the simulation of the conversion between nonactive and active conformations for rifamycin O by rotation of the central part of the ansa chain around the hinge at T13: (a) T13 = 60° (observed in the crystal); (b) T13 = 170° (shortest distance between C34 and the glycolic ring); (c) T13 = 200° (typical for active compounds).

conversion is much easier (about 2 kcal/mol), suggesting that rifamycin O spends most of its time in the conformation found in the crystal. In rifamycin S, whose chemical diagram and crystal structure are shown in Figures 6 and 8(top), respectively, the hindrance of the bulky dioxolanone ring is absent and the rotation around bond C25−C26 presents a single shallow minimum in the range T13 = 80−200° (Figure 5, top, dashed line). Analogue energy profiles calculated for rotation around C17−C18 (T4), Figure 5 (middle), and C19−C20

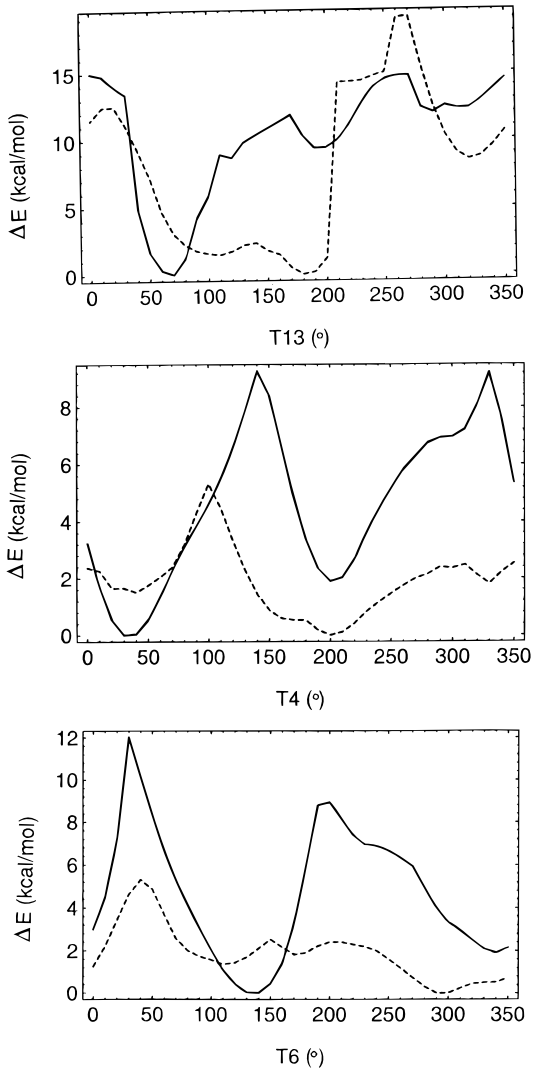

Figure 5. Energy profiles for the rotation of the central part of the ansa chain around the bonds: C26−C27 (T13), C17−C18 (T4), and C19−C20 (T6) for rifamycin O (solid) and rifamycin S (dashed), respectively.

(T6), Figure 5 (bottom), show that for rifamycin O (solid line) the energetic barrier separating the local minima T4 = 40°, T6 = 120° (crystal) and T4 = 180°, T6 = −40° (typical for active compounds) is of the order of 10 kcal/mol, about 2 times larger than for rifamycin S (dashed line).

This suggests that rifamycin O cannot easily adjust the hinge at C19−C20 to facilitate the release of torsional strain on the ansa due to variations in T13. For rifamycin S the rearrangement at C19−C20 involves energies lower than 5 kcal/mol. Thermochemical data support the hypothesis that the dioxolanone ring constrains the molecule in an unfavorable conformation since rifamycin O presents higher internal energy than other rifamycins reflected by the thermochemical data discussed below. In the study of the above conformational conversions, possible cooperative mechanisms involving rearrangements in the central section of the ansa chain have been neglected. This simplification is based on the consideration that the strong intramolecular hydrogen bond involving O9 and O10 is likely to lock the local conformation of the section C20−C24, which in rifamycin O is comparable to active compounds, as

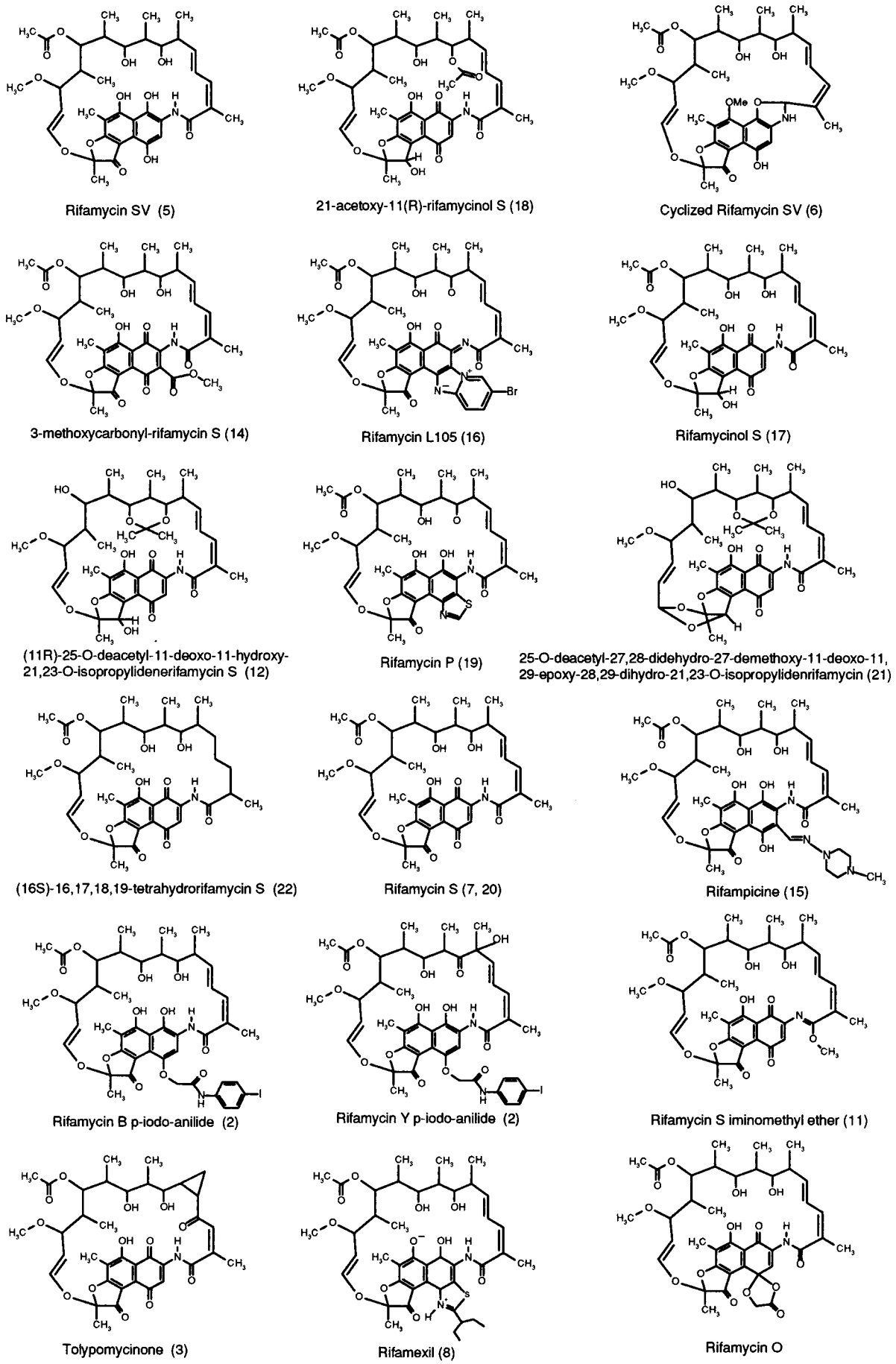

Figure 6. Chemical diagrams of all the rifamycins characterized by X-ray diffraction and used in this work for the Principal Component Analysis. The structures of two polymorphs are known for rifamycin S and rifamexil.

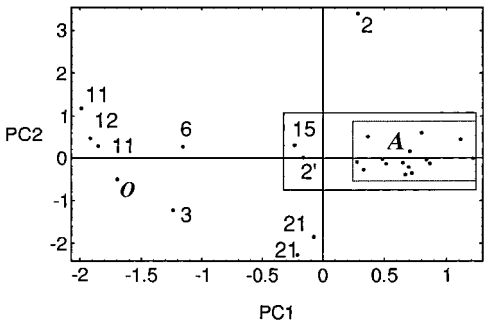

Figure 7. Results of Principal Component Analysis on structural parameters for 26 rifamycins: scatterplot of the scores in the plane defined by the first two principal components. The points are identified according to the numbering of references. Area labeled ***A*** contains compounds described in refs 5, 7, 8 (four molecules), 14, 16, 17 (two molecules), 18, 19 (two molecules), 20, and 22. References 11 and 21 also contain two independent molecules. Reference 2 describes rifamycin Y, nonactive, and rifamycin B, active, labeled with 2 and 2′, respectively. Rifamycin O is indicated as ***O***. It is seen that active compounds cluster in the area indicated with the solid rectangle, while nonactive molecules, apart from 18, are scattered outside.

discussed in the section regarding IR and NMR results.

Structural Parameters Relevant to Activity. The relations between activity and chemical properties of rifamycins have been extensively studied, and a phenomenological model indicating the requirements for activity had been suggested by Lancini and Zanichelli.[1] These are (i) a naphthalene ring carrying oxygens at C1 and C8, either in the quinone or in the hydroquinone form; (ii) two free hydroxyl groups at C21 and C23 on the ansa; (iii) a particular spatial arrangement of the above four oxygens. The model has been refined[5,13,14] by indicating the orientation of O9 and O10 needed for activity. Several structural indicators have been related to activity by different researchers; the most important are torsion angles at the junctions between the chromophore and the ansa, the dihedral angle between the average planes of the chromophore and the ansa, torsion angles involving atoms from C20 to C24, and interatomic O···O distances among O1, O2, O9, and O10.

The qualitative model has been validated by the application of multivariate statistical analysis to structural data.[8] Principal Component Analysis and discriminant function analysis succeeded in discriminating between active and nonactive compounds on the basis of structural data alone.

The use of objective methods to highlight the structural parameters which are relevant for rifamycin activity is further developed in the present work with the aim of obtaining a more accurate model adding one more observation to the 24 different molecular conformations found in 19 rifamycins so far characterized by X-ray diffraction.[15−22] Figure 6 depicts the chemical diagrams of all the structurally known rifamycins. An unbiased description of the molecular conformation has been formulated by considering the 17 torsion angles along the ansa chain backbone, from T1 = C2−N−C15−C16 to T17 = C29−O5−C12−O3, the 6 interatomic distances between the 4 oxygens of the pharmacophore (D1 = O1···O2, D2 = O1···O9, D3 = O1···O10, D4 = O2···O9, D5 = O2···O10, D6 = O9···O10), and the 3 angles between the chromophore and the vector C21−O9 (A1), the chromophore and the vector C23−O10 (A2), and the chromophore and the ansa chain mean planes (A3), respectively. Each molecule corresponds to one point in this 26-dimensional space. Principal Component Analysis was chosen as a useful tool to eliminate redundancy and correlation between parameters, reducing the dimensionality of the problem. (Principal Component Analysis extracts the linear combination of the initial parameters which accounts for the largest fraction of the sample variance (PC1), then the linear combination of parameter, orthogonal to PC1, which accounts for the largest fraction of the residual variance (PC2), and so on until a complete set of new axes is defined. This is equivalent to rotating the initial axis till aligning the first axis to the direction of maximum variance, the second axis to the second largest variance, and so on. The directions accounting for little variance (possibly noise) can then be discarded, and the experimental points are thus projected on the subspace where they are maximally spread. This facilitates the visualization and the process of pattern recognition.[23])

The first two principal components (PC1 and PC2) are sufficient to separate active and nonactive compounds, with the exception of rifamycin O which falls outside the cluster of active molecules. Figure 7 shows the distributions of molecular conformations observed for crystalline rifamycins on the plane described by PC1 and PC2. All the previously characterized active molecules cluster together in the rectangle ($-0.5 < PC1 < 1.5$; $-1 < PC2 < 1$), while all the nonactive compounds are scattered well outside. Apart from rifamycin O, 21-acetoxy-11(*R*)-rifamycinol S[18] is the only misclassified observation. In this case the lack of activity is due to acylation at O9 and not to purely structural reasons. Table 3 reports the coefficients relating PC1 and PC2 to the initial 26 parameters. A factor analysis can be tempted to associate a structural meaning to PC1 and PC2. In fact PC1 is mainly defined by parameters describing the orientation of the central part of the ansa chain relative to the chromophore, namely, T6, T13, T14, D2, D3, D4, and D5, while PC2 is relevantly influenced by parameters defining the local conformation of the central section of the ansa chain, i.e., T7, T8, T10, A1, A2, and D6. The local conformation of the amidic junction does not seem to express any significant pattern, while the conformation of the etheric junction could be correlated to PC1. All but two nonactive rifamycins can be discriminated from active compounds simply because of the different relative orientation of the central part of the ansa chain and the chromophore (separation along PC1), even if the local conformation around O9 and O10 is similar for the two groups (similar PC2). Conversely, despite a suitable orientation at the two nodes C19−C20 and C26−C27 (PC1 falls in the range of active compounds), the lack of activity of rifamycin Y[2] and 25-*O*-deacetyl-27,28-didehydro-27-demethoxy-11-deoxo-11,29-epoxy-28,29-dihydro-21,23-*O*-isopropylidenerifamycin S[21] is due to unfavorable local conformation of the central part of the ansa chain (separation along PC2). In Figure 8 the structural meaning of PC1 and PC2 is visualized by comparing the structure of active rifamycin S (molecule 20 in the Principal Components scatterplot) with those of nonac-

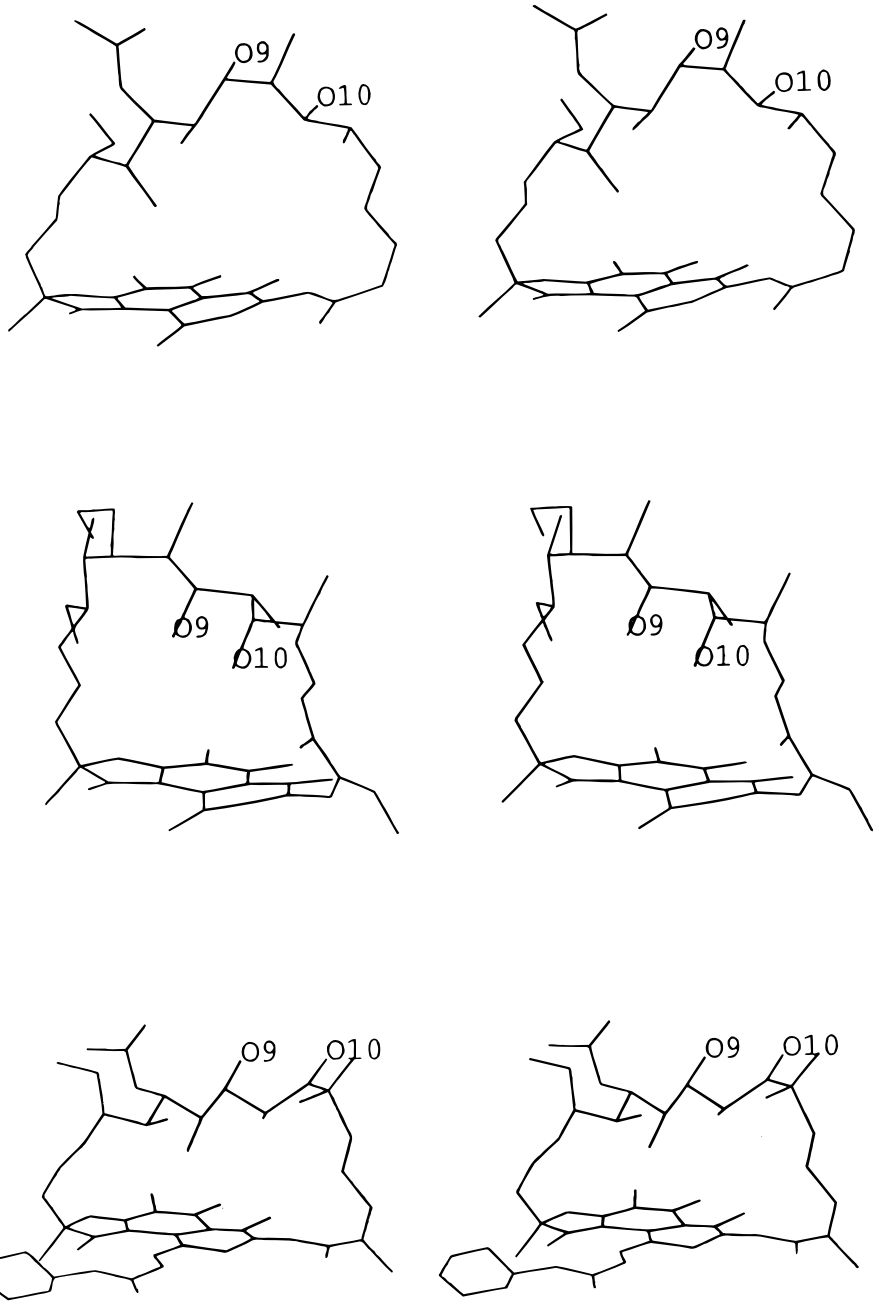

Figure 8. Stereoviews of the molecular structure of rifamycin S (top), rifamycin S iminomethyl ether (middle), and rifamycin Y (bottom). In rifamycin S the orientation of O9 and O10 favors activity. The lack of activity of rifamycin S iminomethyl ether is due to the twisting of the central part of the ansa chain toward the chromophore (distortion along PC1), while for rifamycin Y it is the local conformation around O9 and O10 which prevents activity, with O9 and O10 directed toward opposite sides of the ansa chain (distortion along PC2).

tive rifamycin S iminomethyl ether (molecule 11) and rifamycin Y (molecule 2), which are the most distorted representatives along PC1 and PC2, respectively. Rifamycin O presents a potentially active local arrangement for O9 and O10 (favorable PC2), but the rotations around C19−C20 and C26−C27 determine wrong relative positioning of the four oxygens constituting the pharmacophore (unfavorable PC1). In Figure 9 the superimposition of the structures of all active rifamycins (top) is compared to the conformations of rifamycin S (middle) and rifamycin O (bottom), showing the inward twisting of the central part of the ansa chain differentiating rifamycin O from active compounds.

Mechanism of Oxidation. Rifamycin B exposed to ambient conditions (air, room temperature, and 60% relative humidity) slowly transforms spontaneously into rifamycin O. This oxidation occurs easily, with high yield (about 80%) in solution with oxidizing agents. The process involves nucleophilic attack of the carboxylic terminal oxygen of the glycolic moiety on the sp^2 carbon in position 4 on the naphthalenic group, which then becomes a chiral center. Despite the fact that this attack can occur either from below or from above the naphthalenic plane with respect to the ansa chain, only one diastereoisomer is produced by the oxidation of rifamycin B. X-ray analysis shows that the resulting

Table 3. Loadings on PC1 and PC2 of the 26 Structural Variables Used in Principal Component Analysis[a]

i/*j*	A1	A2	A3	T1	T2	T3	T4	T5	T6	T7	T8	T9	T10	T11	T12	T13	T14	T15	T16	T17	D1	D2	D3	D4	D5	D6
PC1	−0.12	−0.07	0.09	0.17	0.16	0.02	0.19	0.06	−0.30	0.03	0.06	−0.08	0.08	0.15	0.26	0.30	−0.28	0.04	−0.31	0.13	−0.12	0.26	0.32	0.31	0.34	0.05
PC2	−0.23	−0.18	−0.03	−0.17	−0.24	−0.04	−0.04	0.12	0.23	0.33	0.36	−0.01	−0.24	−0.09	−0.16	−0.07	0.22	−0.26	0.05	0.04	−0.21	0.21	0.18	0.15	0.11	0.39

[a] Each principal component is expressed by a linear combination of the initial 26 variables with coefficients C_{ij} reported below, according to: $PCi = \sum_{j=1,26} C_{ij}{*}Var(j)$, with $i = 1, 2$ and $Var(j) =$ A1,..,D6. PC1 is mostly determined by T6, T13, T16, D3, D4, and D5 which affect the conformation of the hinges at C19−C20 and C25−C26. PC2 is determined by the values of T7, T8, and D6 which depend on the conformation of the central section C20−C25.

glycolic ring is oriented nearly perpendicularly to the naphthalenic plane and with the carboxylic group pointing on the same side as the ansa chain, indicating that the attack occurs from above the naphthalenic plane.

To explain the stereospecificity of the oxidation process, the solution structures of rifamycins B and O have been studied by IR and NMR spectroscopy and compared to those of rifamycins S and SV, which differ from the above ones only for the absence of substituents at position 4 (Figure 6).

In Table 4 the ^{1}H NMR assignments of rifamycins O and B obtained in $CDCl_3$ solution are reported, in comparison with those of rifamycins S and SV, respectively**.** In Tables 5 and 6 the vicinal interproton constants of ansa chain for rifamycin O and rifamycin B in comparison with those of rifamycin S and rifamycin SV, respectively, are listed.

As shown in Table 4, the protons involved in significant chemical shift variations ($\Delta\delta \geq 0.15$ ppm) passing from rifamycin S to rifamycin O are H34 ($\Delta\delta = 0.17$ ppm), H26 ($\Delta\delta = 0.61$ ppm), and H24 ($\Delta\delta = -0.41$ ppm). These changes are attributable to the anisotropic effect exerted on the protons of the left part of the ansa chain by the magnetic cone of the lactone carbonyl in the ring originating from the glycolic moiety. It follows that, in agreement with X-ray results, also in solution the dioxolanone ring of rifamycin O must be located on the same side of the ansa chain with respect to the naphthalene ring. Considering now the data in Table 5 concerning the vicinal interproton coupling constants of rifamycin O in comparison with those of rifamycin S, it can deduced from the similarity of the values that the overall ansa chain conformation in the two molecules is very similar and the ansa appears to rock as a unit about pivot points at the ends as suggested by rotation around the 27−28 bond. The IR spectra of rifamycins S and O in $CDCl_3$ solution show the same frequencies for the hydroxyls at C21 (ν(OH) = 3450 cm^{-1}), the OH at C23 (ν(OH) = 3450 cm^{-1}), and the carbonyl of the acetyl group (ν(C═O) = 1707−1708 cm^{-1}). On the basis of these frequencies, it can be deduced that the three groups are intramolecularly hydrogen-bonded[24] and that these molecules show the same hydrogen-bonding strength in this region. This means that they must have a very similar conformation in the C21−C23 region, which in fact is maintained in the solid state. In Table 7 the IR data of rifamycins S and O are compared with those of the inactive rifamycin S iminomethyl ether (shown in Figures 6 and 8, middle) which exhibits the significantly different ν(OH) value at C21 and C23 of 3500 cm^{-1}.

From the comparison of rifamycins B and SV in Table 4, some chemical shift differences (positive or negative) in the ansa chain concerning H21, H33, H25, H26, and H27 reveal that in rifamycin B the glycolic moiety must be located on the same side of the ansa chain with respect to the naphthalene ring. In fact the glycolic moiety can be fixed in this spatial region by the H-bond of the OH of the carboxyl group to the furanone ketone O4 (ν(C═O) = 1675 cm^{-1}) and to O5, while the protons from H21 to H27 along the ansa chain could form a partially positively charged nest capable of accommodating the carboxylic C═O in the left upper part of

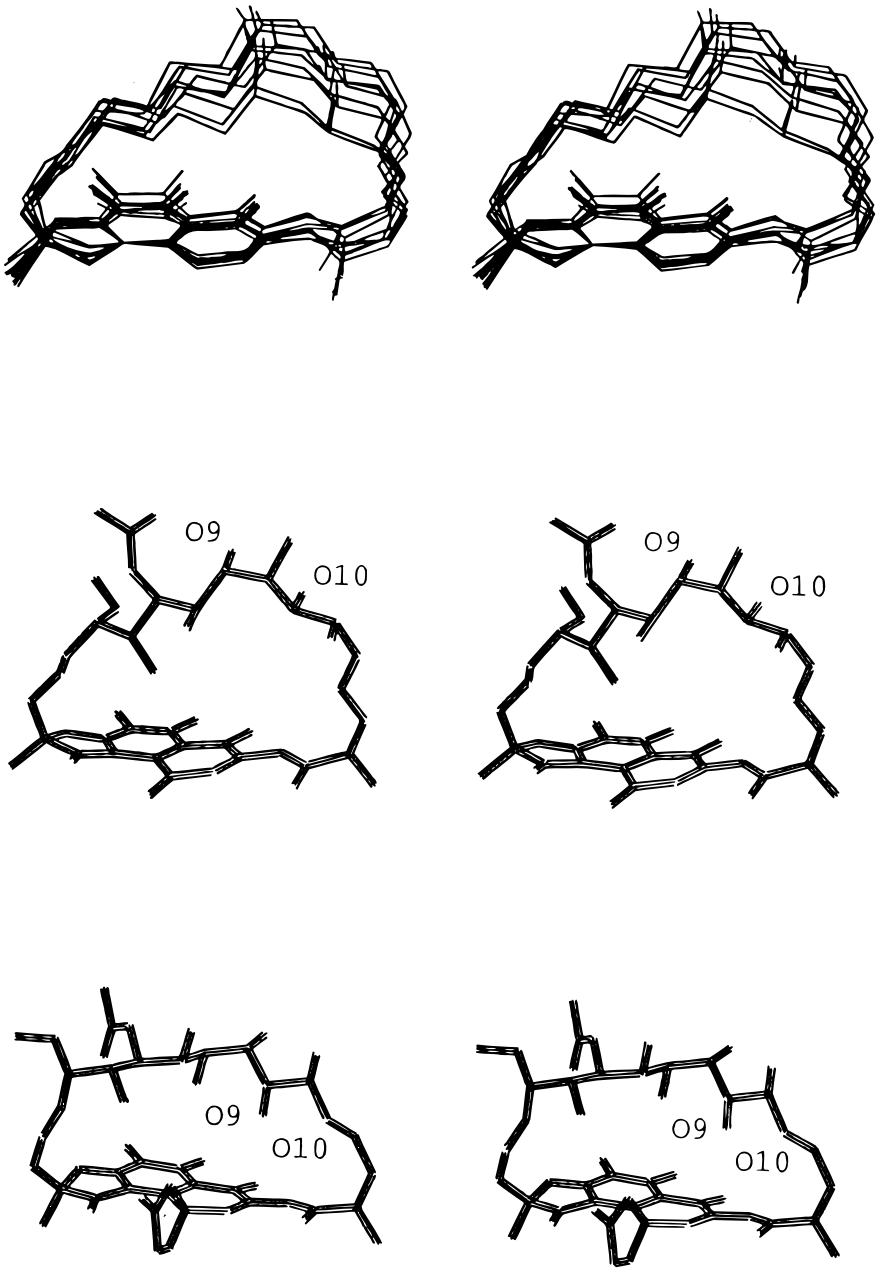

Figure 9. Top: Stereoview of the superimposition of all active rifamycins, the substituents along the ansa chain being omitted for clarity, with the exception of O9 and O10, which belong to the pharmacophore. Middle and bottom: Stereoview of the molecular structures of rifamycin S and rifamycin O, respectively.

the molecule. Since the carboxyl is constrained in this region, the oxidation of rifamycin B produces only the isomer of rifamycin O having the dioxolanone ring in the same region as the ansa chain with respect to the naphthalene ring.

In Table 6 the vicinal interproton coupling constants of rifamycin B in $CDCl_3$ solution are shown to be very similar to those of rifamycin SV confirming that the free glycolic moiety does not induce any change of the ansa conformation. In Table 7 the IR data concerning ν(OH) at C21 and C23 and other absorption frequencies of rifamycin B are compared with those of rifamycin SV and some other active rifamycins (P, rifampicin, rifamexil).

Thermochemical Properties. The heating curve of rifamycin O, reported in Figure 10a, shows a sharp exotherm at 200−220 °C with a peak at 213 °C (ΔH = 79.5 J/g, ΔS = 123.3 J/mol K) related to a well-defined decomposition event. In comparison to the heating curves of other rifamycins (i.e., rifamycin B, Figure 10b, ΔH = 21.1 J/g, ΔS = 36 J/mol K) this behavior is indicative of a high order of the molecules in the crystalline lattice and of a strong intramolecular hydrogen bond system between different groups present in the molecule.

The DSC curve obtained from the crystalline powder does not show any desolvation endotherm in the temperature range from 25 to 120 °C characteristic of imbibition or inclusion solvents always present in all the rifamycin derivatives. This unusual behavior is explained by the fact that the hydrophilic groups present in the molecule are involved in intramolecular contacts which inhibit interactions with solvents.

Table 4. ^{1}H NMR Data of Rifamycin O and Rifamycin B in Comparison with Those of Rifamycin S and Rifamycin SV, Respectively[a]

proton	rifamycin O	rifamycin S	Δ ppm	rifamycin B	rifamycin SV	Δ ppm
$CH_3$16($CH_3$30)	2.03	2.02	0.01	2.10	2.07	0.03
H17	6.18	6.25	−0.11	6.36	6.39	−0.03
H18	6.18	6.31	−0.12	6.36	6.44	−0.08
H19	5.95	5.93	0.1	5.96	6.03	−0.07
H20	2.33	2.27	−0.03	2.45	2.44	0.01
$CH_3$20($CH_3$31)	0.84	0.82	0.02	0.86	0.91	−0.05
H21	3.52	3.55	−0.03	3.68	3.84	−0.16
H22	1.78	1.78	0.00	1.78	1.83	−0.05
$CH_3$22($CH_3$32)	1.01	1.00	0.01	1.06	1.05	0.01
H23	2.99	2.98	0.01	3.03	3.05	−0.02
H24	1.55	1.96	−0.41	1.68	1.60	0.07
$CH_3$24($CH_3$33)	0.69	0.65	0.04	0.60	0.73	−0.13
H25	4.56	4.60	−0.04	4.64	4.88	−0.24
CH_3−C=O	2.03	2.02	0.01	2.05	2.07	−0.02
H26	2.11	1.5	0.61	1.70	1.56	0.14
$CH_3$26($CH_3$34)	0.37	0.20	0.17	−0.20	−0.20	−0.00
H27	3.38	3.37	0.01	3.41	3.55	−0.14
OCH_3	3.13	3.10	0.03	3.09	3.07	0.02
H28	5.1	5.06	0.04	5.04	5.10	−0.06
H29	6.3	6.20	0.10	6.22	6.23	−0.01

[a] From $CDCl_3$ solution at 297 K (chemical shifts and attributions), δ (ppm), TMS as internal standard.

Table 5. Vicinal Interproton Coupling Constants of Rifamycin O in Comparison with Those of Rifamycin S[a]

	J_{13} (Hz)	
proton	rifamycin O	rifamycin S
17,18	nm	8
18,19	14.9	15.4
19,20	7.3	7.0
20,21	9.8	9.8
21,22	≤1	≤1
22,23	nm	2.9
23,24	9.9	10.2
24,25	≤1	1.5
25,26	10.6	10.5
26,27	2.8	2.9
27,28	8.8	7.7
28,29	12.8	12.5

[a] From $CDCl_3$ solution at 297 K. nm, not measured.

Table 6. Vicinal Interproton Coupling Constants of Rifamycin B in Comparison with Those of Rifamycin SV[a]

	J_{13} (Hz)	
proton	rifamycin B	rifamycin SV
17,18	10.2	10
18,19	14.4	14
19,20	5.8	5
20,21	9.5	10
21,22	0	2
22,23	1.5	2
23,24	10.3	nm
24,25	0	1
25,26	10.5	10
26,27	2.3	2
27,28	7.5	7
28,29	12.6	12.5

[a] From $CDCl_3$ solution at 297 K. nm, not measured.

Conclusions

The solution- and solid-state characterization of rifamycin O has been focused on two points: explaining the surprising stereoselectivity of the oxidation of rifamycin B to rifamycin O and elucidating the structure−activity correlation of the latter based on the well-accepted model for the rifamycin pharmacophore. The total stereospecificity of the reaction which converts rifamycin B into rifamycin O is explained on the basis of a conformational preorganization of the glycolic chain in rifamycin B. The crystal structure of rifamycin B[2] has been determined for the *p*-iodoanilide derivative of the glycolic moiety which then presents an extended conformation, coplanar with the naphthalenic ring. Our spectroscopic studies show that when the steric hindrance of the *p*-iodoanilide substituent is removed and

Table 7. Characteristic IR Vibrations of the Groups in the Ansa Chain Involved in the Activity (a) and Others (b−d) in $CDCl_3$ Solution

rifamycin	(a) ν(OH) at C21 and C23	(b) acetyl ν(C=O)	(c) carboxyl ν(C=O)	(d) ν(C11=O)
S	3450	1708		1740
O	3450	1707		1731
S iminomethyl ether	3500	1710		1730
SV	3460	1715		1650
B	3486	1711	1734	1675
P	3480	1712		1655
rifampicin	3480	1715		1640
rifamexil	3470	1710		1645

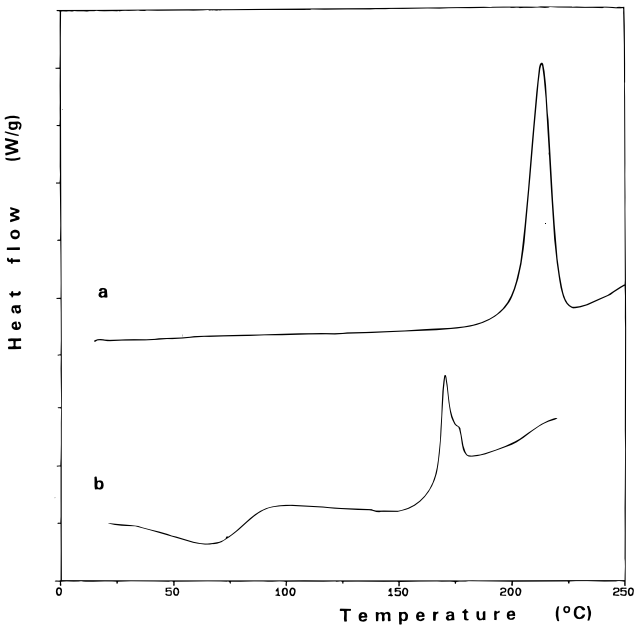

Figure 10. DSC heating curve for (a) rifamycin O and (b) rifamycin B.

Table 8. Quantitative Measures of Activity for the 18 Rifamycins (26 Independent Molecules) Included in the Principal Component Analysis[a]

compound	MIC (μg/mL) *E. coli*	IC_{50} (nM/unit of enzyme) *E. coli*
rifamycin S[7,20]	12[1]	50,[17,22] 40,[34] 85[35]
rifamycin S iminomethyl ether[11]	na[11]	na[11]
cyclized rifamycin SV[6]	na[6]	na[6]
tolypomycinone[3]	na[3]	na[3]
3-(methoxycarbonyl)rifamycin S[14]		20[4]
sodium rifamycin SV[5]	25[1]	85[35]
21-acetoxy-11(*R*)-rifamycinol S[18]	na[18]	na[18]
rifamycin B[2]	100[1]	90[35]
rifamycin Y[2]	na[1]	na[1]
25-*O*-deacetyl-27,28-didehydro-27-demethoxy-11-deoxo-11,29-epoxy-28,29-dihydro-21,23-*O*-isopropylidenerifamycin S[21]	na[21]	na[21]
rifamycin L105[16]	active[16]	
rifamycinol S[17]		50[17]
(11*R*)-25-*O*-deacetyl-11-deoxo-11-hydroxy-21,23-*O*-isopropylidene-rifamycin S[12]	na[12]	na[12]
rifamycin P[19]	3[1], 16[36]	15,[34] 75[35]
rifampicine[4]	20,[33] 8[36]	
(16*S*)-16,17,18,19-tetrahydrorifamycin S[22]		1600[22]
rifamexil[8]	32[36]	
rifamycin O	75[1]	

[a] MIC, minimum inhibitory concentration; and IC_{50}, concentration giving 50% enzyme inhibition. Literature references for the crystal structures are listed along with the compounds. Literature references for activity measures are reported near the corresponding data. na, nonactive.

the carboxyl group restored, the glycolic chain folds preferentially toward the ansa chain due to O−H···O and C−H···O hydrogen bonding. Regarding the oxidation of rifamycin B, this preorientation of the glycolic carboxyl favors the attack on C4 leading to the rifamycin O diastereoisomer found in the crystal structure. By conformational analysis calculations, we have shown that in rifamycin S the methyl group at C34 can swing back and forth in the space between the ansa chain and the chromophore at negligible energetic expense with an oscillation amplitude of about 100°. Due to the intramolecular hydrogen bonds involving O10−H···O9−H···O8, characteristic both in solution and in the solid state, the displacement of C34 is correlated to a rigid rocking of the central part of the ansa chain from C20 to C27. The most favorable position involves a close approach of the methyl to the aromatic moiety, while the bonds C21−O10, C23−O9, and C35−O8 are roughly parallel to the aromatic plane. When the oxolanone ring is formed in the oxidation of rifamycin B to rifamycin O, the energetic profile for the oscillation changes drastically and methyl C34 is confined in a steep minimum far from the naphthalenic ring. The central part of the ansa chain is accordingly rotated, and O8, O9, and O10 point toward the chromophore. A very similar twisting of the central part of the ansa chain around the hinges at C20 and C27 is found in the crystal structure of halomycin B,[25] a naphthalenic ansamycin structural analogue of rifamycins. In that case the steric constraint forcing O9 and O10 toward the chromophore is represented by a water molecule hosted between the chromophore and the ansa chain.

The generally accepted model of the rifamycin pharmacophore[2,5] requires that the bonds C21−O10 and C23−O9 are parallel to the C1−O1 and C8−O2 vectors, as in the crystal structure of rifamycin S. On the basis of multivariate statistical analysis of crystal data and on solution spectroscopic evidence, we have pointed out that the correct reciprocal orientation of O1, O2, O9, and O10 depends on two factors. In the first place a favorable local arrangement of the C20−C27 section of the ansa chain is needed, which is usually granted by the system of intramolecular hydrogen bonds involving O8, O9, and O10. Second, the central part of the ansa chain can rock about the pivot atoms C20 and C27. In the case of rifamycin O the arrangement of O1, O2, O9, and O10 found in the solid state is inconsistent with the pattern characteristic of active compounds, both qualitatively[2,5] and quantitatively (according to multivariate analysis). On the other hand, rifamycin O is reported among active rifamycins by Lancini and Zanichelli.[1] Conformational analysis in solution by ^{1}H NMR vicinal couplings indicates that the ansa chain arrangement of rifamycin O is in large part comparable to the one observed for the active rifamycin S. Nevertheless, a discrepancy is observed around the atom C27, which could correspond to the rocking of the central section of the ansa chain observed in the solid state. The calculation of the energy profile corresponding to the conversion of the molecular conformation observed in the solid state into a conformation similar to rifamycin S shows that this rocking releases the repulsion between the glycolic ring and methyl C34. These findings suggest that the activity observed for rifamycin O could be due either to a chemical transformation of the molecule before reaching the pharmacological target or to an activation of rifamycin O supplying the energy required for conformational rearrangement.

Experimental Section

A pure rifamycin O sample was prepared by the oxidation of rifamycin B and subsequent crystallization process from isopropylic alcohol at room temperature. The purity of the sample was assessed by TLC, elemental analysis, and ^{1}H NMR in $CDCl_3$ solution, while the solvents present in the sample were identified by gas chromatography.

This powder was solubilized in isopropylic alcohol at 60−80 °C, and this solution was kept at room temperature for several days. Crystalline powder with monocrystals was isolated and submitted to solid-state characterization by thermal analysis, thermomicroscopy, and FT-IR spectroscopy.

Thermal analysis was carried out with a DuPont TA 2000 instrument equipped with a DSC cell and TG module. The

working conditions were as follows: gas flow, N_2 at 25 mL/min; heating rate, 10 °C/min; open sample, aluminum pan; sample weight, 3 mg. Thermomicroscopy involved Kofler hot stage microscopy with polarized light. The IR spectrum was recorded with a FT-IR Bruker model IFS 48 spectrophotometer, in Nujol mull and $CDCl_3$ solution.

The ^{1}H NMR spectra (1D and 2D) were recorded by a Bruker DRX 500-MHz instrument at 303 K after the solubilization of the samples in $CDCl_3$ (concentration = 20 mg/mL). The chemical shift values were referred to TMS = 0 ppm.

The assignments of rifamycins O, S, B, and SV are based on the reported data and on 2D COSY spectra.[26]

X-ray Crystallography. Crystal Data for Rifamycin O: $C_{39}H_{47}NO_{14}$, $M = 753.80$, triclinic, $a = 11.823(3)$, $b = 10.397(2)$, $c = 9.501(2)$ Å, $\alpha = 66.95(1)$, $\beta = 104.76(1)$, $\gamma = 115.13(1)°$, $V = 967.4(4)$ Å^3, $T = 293$ K, space group *P1* (no. 1), filtered Cu Kα radiation, $\lambda = 1.541\,78$ Å, $Z = 1$, $D_c = 1.294$ Mg/m^3, $F(000) = 400$, μ(Cu Kα) = 0.8234 cm^{-1}, Siemens AED diffractometer, $\theta-2\theta$ scan, $6 < 2\theta < 140°$, 3677 measured reflections, 3677 unique reflections, 3151 unique observed reflections ($I > 2\sigma(I)$). The phase problem was solved by direct methods (SIR92[27]), and the structure was refined by full-matrix least-squares on all measured F_o^2 with SHELXL93.[28] Anisotropic thermal displacement parameters were refined for all non-hydrogen atoms. Hydrogens bonded to O2, O9, and O10, considered important for the definition of the pharmacophore, were located by inspection of the ΔF map and refined isotropically. The remaining H atoms were introduced at calculated positions, riding on their carrier atoms, according to the protocols built in the refinement program.

Final refinement on 510 parameters gave $R_1 = 0.056$ (on observed data), $R_1 = 0.065$ (on all data), $wR_2 = 0.166$, gof = 1.118. Final difference Fourier map was featureless. Programs PARST95,[29] ZORTEP,[30] and PLUTO[31] were used for analyzing and drawing molecular structures and crystal packing.

All the calculations were performed on an ENCORE91 computer of the Centro di Studio per la Strutturistica Diffrattometrica del CNR in Parma.

Statistical Analysis of Structural Data. The Cambridge Structural Database[32] was searched to retrieve structural data for all rifamycins characterized by X-ray diffraction.[11,12,14−22] In some cases[6,16] coordinates were not deposited and were kindly provided by authors. To these (16 active, 9 nonactive), data concerning rifamycin O were added, for a total of 26 independent molecules. Table 8 reports quantitative measures of in vitro activity taken from literature for the compounds included in the analysis. In the course of the analysis we found that three rifamycins (five independent molecules) appear in the literature and in the Cambridge Structural Database with the wrong absolute configuration, seriously affecting the discussions based on torsion angles. In the present work all values have been revised and fixed. Principal Component Analysis has been performed on a set of 26 *Z*-scaled structural variables (defined in the Results and Discussion) by the SAS package.[37] Calculations were performed on RISC/6000 and Silicon Graphics workstations of the Centro di Calcolo Elettronico at the University of Parma.

Molecular Modeling. The energies for the rearrangements of torsion angles C16−C17−C18−C19 (T4), C18−C19−C20−C21 (T6), and C25−C26−C27−C28 (T13) have been evaluated. The crystal structures of rifamycin O and rifamycin S[20] have been used as starting models. Intramolecular hydrogen bonds observed in the solid state have been preserved; the remaining hydrogens have been placed at typical positions, according to the geometry of their carrier atoms. Energy profiles have been calculated by the program Sybyl,[38] using the standard Tripos force field. Each profile corresponds to the energy variations accompanying the modifications of T4, T6, and T13, respectively. The rearrangement paths have been divided into 35 steps of 10°; in each case the initial value was chosen to be about 10−20° away from the value found in the crystal. After updating the torsion angle involved in the rearrangement, the molecular geometry was optimized to release structural strains; the starting conformation was taken from the previous step. Electrostatic contribution has been included in the calculations, with cutoff radius of 16 Å and $\epsilon_r = 1.5$ (independent from distance). Different protocols for evaluating atomic partial charges have been explored, with the aid of Gaussian92.[39] Values given by the Gesteiger and Marsili method[40] and values derived by Mulliken's analysis performed on the results of ab initio single-point calculations using STO-3G and 321-G basis sets were found in relevant disagreement each other. This prompted us to use the more robust method of potential derived charges,[41] as implemented in Gaussian92, in which atomic charges are optimized in order to best reproduce the electrostatic potential derived by ab initio calculation and to fit the molecular dipole moment. STO-3G basis set was used. The program Sybyl was run on a Silicon Graphics workstation, while Gaussian92 was run on a CRAY T3Dv at CINECA, Bologna, Italy.

Supporting Information Available: Listings of anisotropic thermal displacement parameters, hydrogen coordinates, and torsion angles for the X-ray crystal structure of rifamycin O (12 pages). Ordering information is given on any current masthead page.

References

(1) Lancini, G.; Zanichelli, W. Structure−activity relationship in rifamycins. In Structure−activity relationship among the semisynthetic antibiotics; Perlman, D., Ed.; Academic Press: New York, 1977; pp 531−600.

(2) Brufani, M.; Cerrini, S.; Fedeli, W.; Vaciago, A. Rifamycins: an insight into biological activity based on structural investigations. *J. Mol. Biol.* **1974**, *87*, 409−435.

(3) Brufani, M.; Cellai, L.; Cerrini, S.; Fedeli, W.; Vaciago, A. Structure−activity relationships in the ansamycins: the crystal structure of tolypomycinone. *Mol. Pharmacol.* **1978**, *14*, 693−703.

(4) Brufani, M.; Cellai, L.; Cerrini, S.; Fedeli, W.; Segre, A.; Vaciago, A. Molecular structure and activity of 3-carbomethoxy rifamycin S. *Mol. Pharmacol.* **1982**, *21*, 394−399.

(5) Arora, S. K. Correlation of structure and activity in ansamycins: molecular structure of sodium rifamycin SV. *Mol. Pharmacol.* **1983**, *23*, 133−140.

(6) Arora, S. K.; Main, P. Correlation of structure and activity in ansamycins: molecular structure of cyclized rifamycin SV. *J. Antibiot.* **1984**, *37*, 178−181.

(7) Arora, S. K. Correlation of structure and activity in ansamycins: structure, conformation and interactions of antibiotic rifamycin S. *J. Med. Chem.* **1985**, *28*, 1099−1102.

(8) Bacchi, A.; Mori, G.; Pelizzi, G.; Pelosi, G.; Nebuloni, M.; Panzone, G. B. Polymorphism-structure relationships of rifamexil, an antibiotic rifamycin derivative. *Mol. Pharmacol.* **1995**, *47*, 611−623.

(9) Buergi, H. B.; Dunitz, J. D. From crystal statics to chemical dynamics. *Acc. Chem. Res.* **1983**, *16*, 153−161.

(10) Klebe, G. The use of crystal data together with other experimental and computational results to discuss structure−reactivity and activity relationships. *Struct. Chem.* **1990**, *1*, 597−616.

(11) Arora, S. K. Structural investigations of mode of action of drugs. III. Structure of rifamycin S iminomethyl ether. *Acta Crystallogr. Sect. B* **1981**, *37*, 152−157.

(12) Bartolucci, C.; Cellai, L.; Cerrini, S.; Lamba, D.; Segre, A. L.; Brizzi, V.; Brufani, M. 21. Synthesis, reactivity studies, and X-ray crystal structure of (11*R*)-25-*O*-deacetyl-11-deoxo-11-hydroxy-21,23-*O*-isopropylidenerifamycin S. *Helv. Chim. Acta* **1990**, *73*, 185−198.

(13) Cellai, L.; Cerrini, S.; Segre, A.; Brufani, M.; Fedeli, W.; Vaciago, A. Comparative study of the conformations of rifamycins in solution and in the solid state by Proton Nuclear Magnetic Resonance and X-rays. *J. Org. Chem.* **1982**, *47*, 2652−2661.

(14) Cellai, L.; Cerrini, S.; Segre, A.; Brufani, M.; Fedeli, W.; Vaciago, A. A study on the structures of 3-methoxycarbonylrifamycins by X-ray crystallography and ^{1}H nuclear magnetic resonance spectroscopy. *J. Chem. Soc., Perkin Trans. 2* **1982**, 1633−1640.

(15) Gadret, M.; Goursolle, M.; Leger, J. M.; Colleter, J. C. Structure cristalline de la rifampicine. *Acta Crystallogr. Sect. B* **1975**, *31*, 1454−1462.

(16) Brufani, M.; Cellai, L.; Cerrini, S.; Fedeli, W.; Marchi, E.; Segre, A.; Vaciago, A. X-ray crystal structure of 4-deoxy-3′-bromopyrido-[1′,2′-1,2]imidazo[5,4-c] rifamycin S. *J. Antibiot.* **1984**, *37*, 1623−1627.

(17) Cellai, L.; Cerrini, S.; Lamba, D.; Brizzi, V.; Brufani, M. X-ray crystal structure and activity of rifamycinol, a semi-synthetic derivative of the antibacterial antibiotic rifamycin S showing a dimeric $\pi-\pi$ complex in the crystal. *J. Chem. Res. (S)* **1987**, 328−329.
(18) Cerrini, S.; Lamba, D.; Burla, M. C.; Polidori, G.; Nunzi, A. Structure of 21-acetoxy-11(*R*)-rifamycinol S. The role of the one- and two-phase semi-invariants in multisolution phasing methods. *Acta Crystallogr. Sect. C.* **1988**, *44*, 489−495.
(19) Leger, J. M.; Carpy, A. 31. Structure cristalline d'une thiazolorifamycine: rifamycine P. *Helv. Chim. Acta* **1991**, *74*, 326−330.
(20) Arora, S. K.; Arjunan, P. Molecular structure and conformation of rifamycin S, a potential inhibitor of DNA-dependent RNA polymerase. *J. Antibiot.* **1992**, *45*, 428−431.
(21) Bartolucci, C.; Cellai, L.; Cerrini, S.; Di Filippo, P.; Lamba, D. 11. X-ray crystal structure of 25-*O*-deacetyl-27,28-didehydro-27-demethoxy-11-deoxo-11,29-epoxy-28,29-dihydro-21,23-*O*-isopropylidenrifamycin S. *Helv. Chim. Acta* **1992**, *75*, 153−159.
(22) Bartolucci, C.; Cellai, L.; Cerrini, S.; Di Filippo, P.; Lamba, D.; Segre, A. L.; Bianco, A. D.; Guise, M.; Pasquali, V.; Brufani, M. Hydrogenation of the ansa-chain of rifamycin. X-ray crystal structure of (16S)-16,17,18,19-tetrahydrorifamycin S. *Helv. Chim. Acta* **1993**, *76*, 1459−1468.
(23) Murray-Rust, P.; Raftery, J. Computer analysis of molecular geometry. Part VI: classification of differences in conformation. *J. Mol. Graphics* **1985**, *3*, 50−59.
(24) Ferrari P.; Gallo, G. G. *Farmaco Ed. Sci.* **1975**, *30*, 676−696.
(25) Arora, S. K.; Kook, A. M. Structure and conformation of halomycin B in solid state and solution. *J. Org. Chem.* **1987**, *52*, 1530−1535.
(26) Martinelli, G.; Gironi, P.; Gallo, G. G. Conformation, hydrogen bonding, ionization of various rifamycins in nonaqueous and aqueous solutions as studied by H−NMR spectroscopy. *Farmaco Ed. Sci.* **1981**, *36*, 671−681.
(27) Altomare, A.; Cascarano, G.; Giacovazzo, C.; Guagliardi, A.; Burla, M. C.; Polidori, G.; Camalli, M. SIR92. A program for automatic solution of crystal structures by direct methods. *J. Appl. Crystallogr.* **1994**, *27*, 435.
(28) Sheldrick, G. SHELXL93, Program for structure refinement; University of Goettingen: Germany, 1993.
(29) Nardelli, M. PARST95. An update to PARST: a system of Fortran routines for calculating molecular structure parameters from the results of crystal structure analyses. *J. Appl. Crystallogr.* **1995**, *28*, 659.
(30) Zsolnai, L.; Pritzkow, H. ZORTEP, ORTEP original program modified for PC; University of Heidelberg: Germany, 1994.
(31) Motherwell, W. D. S.; Clegg, W. PLUTO, Program for plotting molecular and crystal structures; University of Cambridge: England, 1976.
(32) Allen, F. H.; Kennard, O. Cambridge Structural Database. *Chem. Des. Automation News* **1993**, *8*, 1 and 31−37.
(33) Bartolucci, C.; Cellai, L.; Martuccio, C.; Rossi, A.; Segre, A. L.; Rizera Savu, S.; Silvestro, L. 136. Synthesis of glycosylrifamycins, a new type of semisynthetic rifamycins. *Helv. Chim. Acta* **1996**, *79*, 1611−1619.
(34) Dampier, M. F.; Whitlock, H. W., Jr. Electronegative groups at C-3 of rifamycin S enhance its activity toward DNA-dependent RNA polymerase. *J. Am. Chem. Soc.* **1975**, *97*, 6254−6256.
(35) Wherli, W.; Stahelin, M. The rifamycins relation of chemical structure and action on RNA polymerase. *Biochem. Biophys. Acta* **1969**, *182*, 24−29.
(36) Cavalleri, B.; Turconi, M.; Tamborini, G.; Occelli, E.; Cietto, G.; Pallanza, R.; Scotti, R.; Berti, M.; Romanò, G.; Parenti, F. Synthesis and biological activity of some derivatives of rifamycin P. *J. Med. Chem.* **1990**, *33*, 1470−1476.
(37) SAS; SAS Institute Inc.: Cary, NC, 1989.
(38) SYBYL 6.3; TRIPOS Assoc. Inc.: St. Louis, MO, 1991−1996.
(39) Frisch, M. J.; Trucks, G. W.; Head-Gordon, M.; Gill, P. M. W.; Wong, M. W.; Foresman, J. B.; Johnson, B. G.; Schlegel, H. B.; Robb, M. A.; Replogle, R. S.; Gomperts, R.; Andres, J. L.; Raghavachari, K.; Binkley, J. S.; Gonzalez, C.; Martin, R. L.; Fox, D. J.; Defrees, D. J.; Baker, J.; Stewart, J. J. P.; Pople, J. A. Gaussian92; Gaussian, Inc.: Pittsburgh, PA, 1992.
(40) Gesteiger, J.; Marsili, M. Iterative partial equalization of orbital electronegativity. A rapid access to atomic charges. *Tetrahedron* **1980**, *36*, 3219−3288.
(41) Tomasi, J.; Bonaccorsi, R.; Cammi, R. The extramolecular electrostatic potential. An indicator of the chemical reactivity. In *Theoretical Models of Chemical Bonding, IV*; Maksic, Z. B., Ed.; Springer-Verlag: Berlin, 1990.

JM970791O